ACS OMEGA

http://pubs.acs.org/journal/acsodf

Article

Laser-Induced Graphene Derived from Kraft Lignin for Flexible Supercapacitors

Faisal Mahmood, Hanwen Zhang, Jian Lin, and Caixia Wan*

Cite This: *ACS Omega* 2020, 5, 14611−14618

Read Online

ACCESS | Metrics & More | Article Recommendations | Supporting Information

ABSTRACT: Porous graphene was photothermally induced from kraft lignin via direct laser writing. This laser-induced graphene (LIG) possessed a hierarchical structure with a three-dimensional (3D) interconnected network ideal for its transfer from the kraft lignin/poly(ethylene oxide) (KL/PEO) film onto polydimethylsiloxane (PDMS). The resultant LIG/PDMS composite was shown to keep the intrinsic porous structure and electrically active sites of LIG. The supercapacitors (SCs) fabricated using the LIG/PDMS composite exhibited good electrochemical performance and excellent cyclic stability. More than 90% capacitance was retained after 10 000 cycles. Moreover, due to their high flexibility, the SCs were able to endure bending deformation without significantly sacrificing their capacitance. The proposed technology for the fabrication of flexible SCs based on lignin-derived LIG demonstrated great potential to use a low-cost, renewable material for the manufacture of portable and wearable electronics.

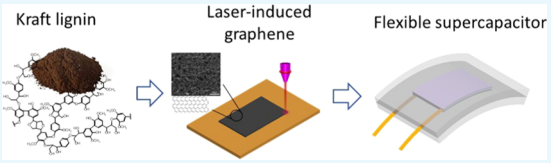

INTRODUCTION

Flexible energy storage devices have attracted great attention for their applications in highly demanded portable and wearable electronics.[1] Supercapacitors (SCs), as one of the most effective and practical technologies for energy storage, have been intensively explored for wearable electronics.[1,2] SCs bridge the power/energy gap between batteries and conventional dielectric capacitors by offering a number of distinct benefits, such as short charge time, high power density, and long cycle life.[2] The energy storage mechanisms of SCs can be associated with either reversible faradic reactions or electrostatic charge accumulation at the interface of electrolyte/electrode.[3] The latter mechanism defines electrical double-layer capacitors (EDLCs) whose capacitance strongly depends on the accessibility of electrodes to electrolytic ions.[3] This also becomes one of the criteria for electrode selection for EDLCs. As the most common electrode materials, carbon electrodes have been widely used for SCs.[4] However, many carbon electrodes are still limited in capacitance and conductivity as well as chemical stability. Therefore, great research efforts have been made to improve the electrochemical performance of carbon electrodes by developing novel structures, such as three-dimensional (3D) hierarchical porous carbon and two-dimensional (2D) carbon nanosheet (i.e., graphene).[3,5,6] Such structures facilitate mass and charge transport by shortening their diffusion paths and thus contribute to the increased capacitance of EDLCs.

Graphene is an exotic 2D carbon nanomaterial possessing attractive physicochemical properties and intrinsic electrical double-layer capacitance due to its unique sp^2 network carbon structure.[7] It has gained extensive research interest for SCs and many other applications.[7] However, the complex synthesis of graphene involving high temperature or tedious chemical processes hinders its mass production for large-scale application.[8,9] Recently, laser-induced graphene (LIG), a porous graphene material, has been emerging for a number of applications due to its facile and scalable synthesis.[10] LIG is synthesized via a one-step and ultrafast laser treatment, the so-called direct laser writing (DLW), under ambient condition.[11,12] Moreover, the physicochemical properties of LIG can be tailored by regulating the DLW parameters and atmosphere. LIG has been shown to exhibit high performance in supercapacitors (SCs), physical/chemical sensors, and electrocatalysts, just to name a few.[10] This suggests the great potential of LIG as a platform nanomaterial for numerous commercial applications. In the context of wearable electronics,[13,14] LIG transferred onto polydimethylsiloxane (PDMS) has been shown to act as flexible and soft electrodes for strain sensing and energy storage.[15−17] Transferring LIG onto an elastomeric substrate overcomes the weak adherence of LIG to a carbon precursor and would allow multifunctional applications with improved robustness in device fabrication.

LIG can be synthesized from both synthetic polymers and renewable materials. Among diverse carbon precursors, biomass has been regarded as a low-cost and renewable precursor for LIG production.[10,18−20] Lignin is proposed to be the most favorable constituent in lignocellulosic biomass for LIG formation due to its high carbon content and abundant

Received: March 23, 2020
Accepted: May 25, 2020
Published: June 9, 2020

https://dx.doi.org/10.1021/acsomega.0c01293
ACS Omega 2020, 5, 14611−14618

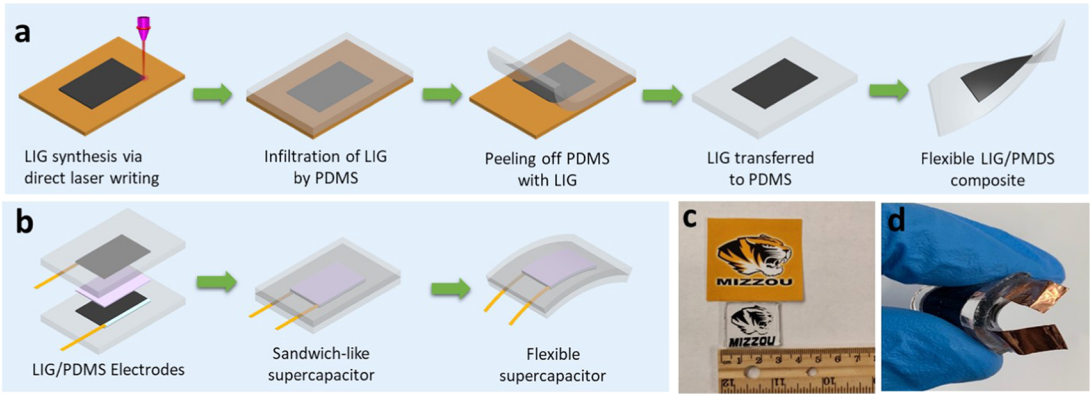

Figure 1. Schematic diagram for LIG synthesis from kraft lignin and fabrication of flexible SC. (a) LIG formation on the kraft lignin/poly(ethylene oxide) (KL/PEO) film via DLW and LIG transfer onto PDMS. (b) Fabrication of a flexible supercapacitor using LIG/PDMS composite and H_2SO_4/poly(vinyl alcohol) (PVA) as a gel electrolyte. (c) LIG/PDMS patterned with MIZZOU Tiger logo. (d) Optical image of a flexible SC.

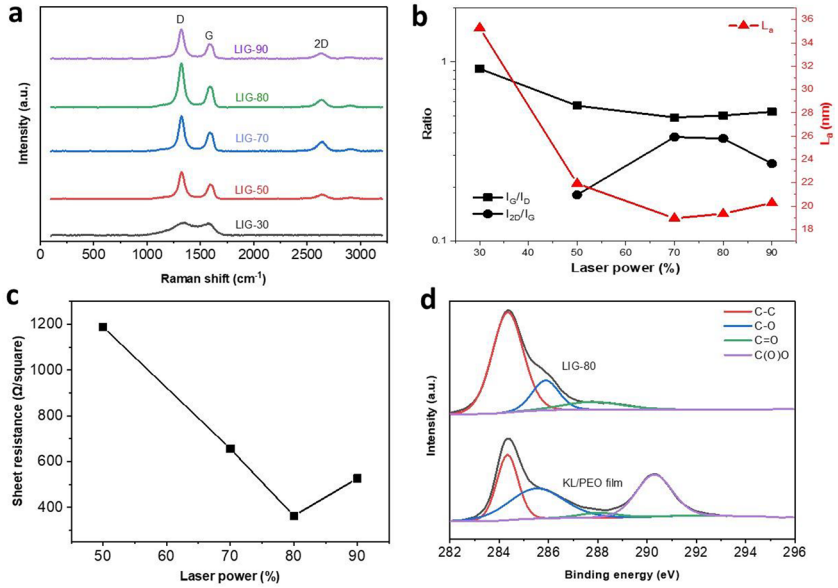

Figure 2. Characterization of LIG. (a) Raman spectra of LIG obtained at different laser powers. (b) Ratios of I_G/I_D and I_{2D}/I_G as well as average crystalline size (La) of LIG obtained at different laser powers. (c) Sheet resistance of LIG obtained at different laser powers. (d) High-resolution C 1s XPS spectra of LIG-80 and KL/PEO film.

aromatic subunits.[18,20] On the other hand, lignin is generated as a waste byproduct in large quantities in pulp mills and biorefinery facilities.[21] Such pulping/pretreatment byproduct, the so-called technical lignin, entails value-added use to make biorefinery/pulp mills profitable. Therefore, the lignin-to-LIG concept would not just enable renewable graphene production but also open a new avenue to lignin valorization in a cost-effective way. However, research on lignin transformation into LIG is limited. An early attempt on converting alkaline lignin into LIG resulted in mixed amorphous and graphitic carbon.[18] Recent studies reported that LIG can be synthesized from lignin-based composite films, which demonstrates good electrochemical performance for SCs.[22−24] However, compared to polyimide (PI)-based LIG, lignin-based LIG remains largely underexplored. Given the renewability and low cost of lignin as well as its structural suitability for LIG synthesis, it is worthy to further the applications of lignin-derived LIG. To this end, one area to explore is emerging flexible/wearable electronics, especially for next-generation energy storage and healthcare/medical devices.[13]

In this work, kraft lignin was used as a carbon precursor for LIG synthesis. Since kraft pulping dominates the pulp and paper industry, kraft lignin is generated in a large quantity (~40 million tons/year), accounting for more than 1/3 of the total amount of technical lignin generated in pulp and biorefinery industries.[25] Although kraft lignin has been investigated for aromatic production and material fabrication,[25−27] cost-effective upgrading routes have not been realized yet due to its recalcitrant structure. Upgrading kraft lignin into porous graphene as demonstrated in the present work would point to a new direction. Here, LIG was synthesized from kraft lignin via DLW (Figure 1), which was well identified via a series of characterization techniques. Moreover, soft electrodes were fabricated by transferring kraft lignin-derived LIG onto PDMS and subsequently used for flexible SCs. The fabricated SCs showed good electrochemical performance.

https://dx.doi.org/10.1021/acsomega.0c01293
ACS Omega 2020, 5, 14611−14618

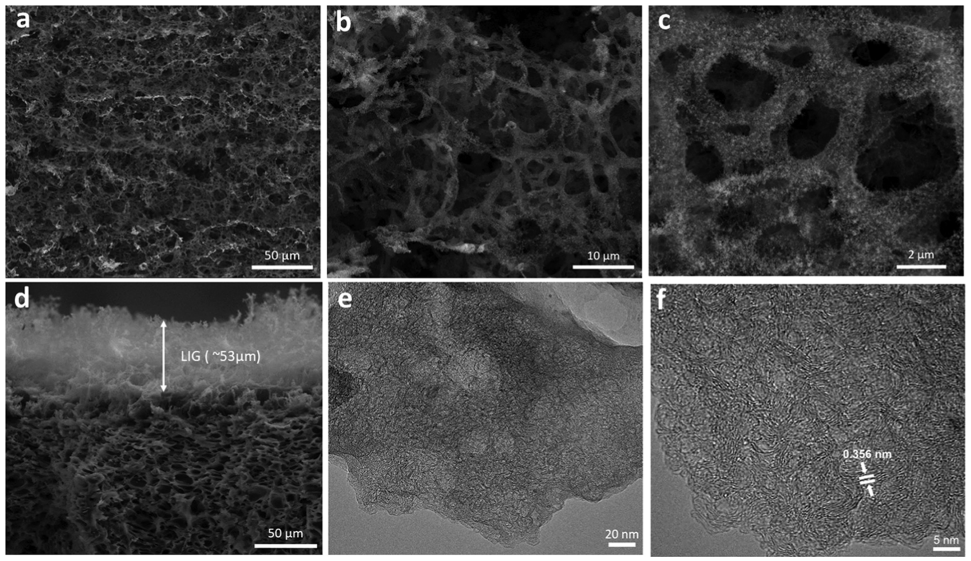

Figure 3. Electron microscopy analysis of LIG-80. (a) SEM image; scale bar is 50 μm. (b, c) SEM images at high magnification; scale bars are 10 and 2 μm, respectively. (d) Cross-sectional SEM image; scale bar is 50 μm. (e, f) HRTEM images; scale bars are 20 and 5 nm, respectively.

RESULTS AND DISCUSSION

LIG Characterization. We first investigated the effects of different laser power on graphene formation. In Raman spectra (Figure 2a), three dominant peaks were observed with LIG fabricated at a power level of 50% or above: a D peak at ~1350 cm^{-1} induced by defects and bending of sp^2 carbon bonds, a G peak at ~1580 cm^{-1} from first-order Raman band of all sp^2-hybridized carbon, and a 2D peak from second-order zone-boundary phonons.[28] The I_{2D}/I_G ratio increased with the increase in laser power from 50 to 70% and then slightly decreased when the power level was increased to 80% (Figure 2b). A further increase in power level to 90% caused a significant decrease in the I_{2D}/I_G ratio, indicating the deteriorated quality of graphene due to severe photothermal effects caused by strong laser power. A similar effect of laser power was also observed with other carbon precursors (e.g., wood, PI film, and lignin).[18,24] The I_G/I_D ratio decreased with the power level up to 70% and then slightly increased with a further increase in laser power. A higher laser power level did not necessarily lead to suppressed D peak most likely due to the highly oxidized lignin/PEO film and the highly functionalized, oxygen-rich structure of lignin.[18,24] The average crystalline size (La) followed a similar trend to the I_G/I_D ratio, which ranged from 19−22 nm for laser power above 30%. Overall, 80% laser power appeared to be the optimal level to induce LIG with a higher quality. This was also evidenced by sheet resistance (Rs) of LIG-80, which gave the lowest value (363.1 Ω/square) (Figure 2c). In contrast, LIG obtained at the other effective power levels (50, 70, and 90%) showed much higher Rs, and the pristine KL/PEO film and the film scribed at 30% power level were basically an insulator (with Rs above 200 MΩ).

LIG-80 was further characterized for morphology and micro/ultrastructure using electron microscopy. Scanning electron microscopy (SEM) images showed a foamlike porous structure (Figure 3a), which is typical to LIG fabricated from various carbon precursors.[12] The rapid release of gaseous molecules generated during laser scribing led to the formation of such a hierarchical porous structure.[11,12] A closer look at the carbon matrix by SEM at high magnification revealed the beehive-like structure with porosity down to nanoscale (Figure 3b,c). Moreover, as shown in the cross-sectional SEM image (Figure 3d), the porous structure was present in a forest-like shape, with the LIG layer protruding from the KL/PEO film with a thickness of ~53 μm. Such hierarchical porous structure is beneficial for the electrochemical performance as it can facilitate fast diffusion of electrolyte into electrode due to enhanced accessible surface area.[11] High-resolution transmission electron microscopy (HRTEM) images show fringe-like patterns of LIG with a *d*-spacing of 0.356 nm characteristically for the distance of two neighboring graphitic carbons (Figure 3e,f), indicating the presence of graphene. These graphene patterns are responsible for LIG's high electrochemical activity and low sheet resistance.

The chemical composition of LIG-80 was determined by XPS. The pristine lignin film contained three major elements, i.e., C, O, and Na (Figure S2a), of which Na was primarily from the NaOH solution used to dissolve kraft lignin for film fabrication. Laser writing led to an increase in carbon content, which was more than double that in the pristine lignin film (Figure S2a). Moreover, oxygen was suppressed by laser writing. It was interesting to note that laser writing led to a more than 3-fold decrease in the Na content. The compositional changes in response to laser writing suggested that photochemical reaction could also occur along with the photothermal reaction during the DLW process. High-resolution C 1s spectra revealed four major functionalities (Figure S2b): sp^2 C−C bond at 284.4 eV, C−O at 285.7 eV, C═O at 288.5 eV, and O−C═O bond at 290.5 eV. Compared to the pristine lignin film, LIG-80 had a significantly increased sp^2 C−C bond, accounting for 71.55% of the C 1s major functionalities. In addition, LIG-80 had no O−C═O bond and a reduced content of the C−O bond. The change of C 1s functionality, especially the increase in sp^2 C−C, indicated that laser scribing resulted in graphitization of lignin, further corroborating the HRTEM and Raman results.

Infiltration of LIG for the LIG/PDMS Electrode. To enable the fabrication of the highly flexible LIG electrode derived from kraft lignin, we attempted to transfer the derived LIG onto an elastomeric substrate, i.e., PDMS. Figure 1a

https://dx.doi.org/10.1021/acsomega.0c01293
ACS Omega 2020, 5, 14611−14618

depicts the process of transferring LIG from the KL/PEO film onto PDMS. As shown in Figure 4a–c, LIG was successfully

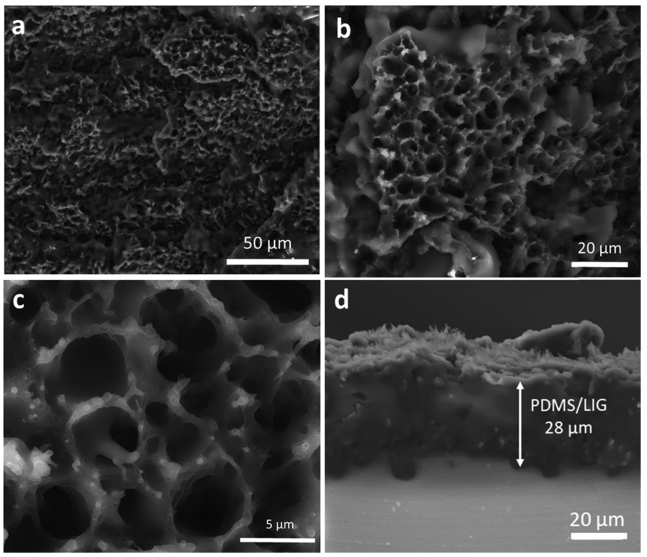

Figure 4. SEM images of LIG-80 transferred to PDMS, namely, LIG-80/PDMS. (a–c) Top views at different magnifications; scales bars are 50, 20, and 5 μm, respectively. (d) Cross-sectional view (back-scattered); scale bar is 20 μm.

transferred onto PDMS, with original hierarchical structures of LIG largely retained on PDMS. This suggested that the porous interconnected network of LIG, as presented in Figure 3a, would be beneficial to the infiltration of LIG by PDMS. It should be noted that a complete transfer of LIG was not achieved, leaving some LIG attached to the original lignin film (Figure S3). The cross-sectional SEM images showed that the LIG-embedded PDMS layer had a thickness of ~28 μm and a porous structure (Figure 4d). This led us to believe that the porous PDMS structure would allow a gel electrolyte to seep into the pores and contact embedded LIG. The connection between transferred LIG and gel electrolyte completed the circuit for an SC device, as discussed in a later section.

Electrochemical Performance of the LIG/PDMS Electrode for Flexible SCs. A flexible SC was fabricated using the LIG-80/PDMS composite as both electrode and current collector. The cyclic voltammetry (CV) curves of the SC at various scan rates are shown in Figure 5a. With the scan rate increased from 10 to 500 mV s^{-1}, the CV curves of LIG-80/PDMS-SC still remained pseudorectangular, indicating the typical capacitive behavior of electric double layers (Figure 5a). The device had the maximum areal capacitance (C_A) of 880 μF cm^{-2} (with the corresponding C_V of 314 μF cm^{-3}) at a scan rate of 10 mV s^{-1} (Figure 5b). The specific capacitance decreased with an increase in scan rate, which can be attributed to reduced diffusion of ions into PDMS pores and their insufficient contact with the LIG electrode at a higher scan rate.[29] Nevertheless, at similar scan rates, the C_A value was higher than that of stretchable and flexible SCs fabricated using graphene/PDMS (up to 840 μF cm^{-2}) (Table S1).[30−32] Elastomeric SCs based on LIG were also reported,[17,33] but with carbon precursor limited to PI. Compared to the counterparts based on PI-derived LIG, the SCs fabricated here also showed higher C_A values. It should be noted that the maximum C_A of the aforementioned graphene-/LIG-based SCs required gold deposition[31] or nitrogen doping.[33] Our findings based on pristine LIG derived from KL suggested high potential of such LIG for soft electrodes with good electrochemical performance. The CD curves of the device were near-triangular (Figure 5c), further confirming the effective ion deposition on the interface of electrolyte and electrode. Similar to the CV analysis, C_A as a function of current density decreased with an increase in current density. The C_A value decreased to almost half when the current density was doubled. The maximum CD-based C_A was 2.51 mF cm^{-2}, further demonstrating its high capacitance compared to the reported SCs, as discussed above. The energy and power

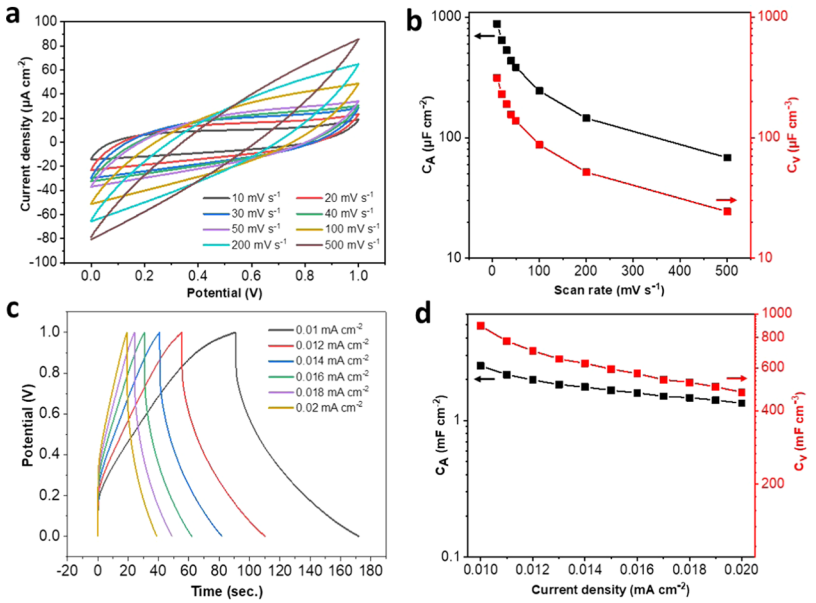

Figure 5. Electrochemical analysis of LIG-80/PDMS-SC. (a) CV curves obtained at different scan rates. (b) Specific areal and volumetric capacitances as a function of scan rate. (c) CD curves obtained at different current densities. (d) Specific areal and volumetric capacitances as a function of current density.

https://dx.doi.org/10.1021/acsomega.0c01293
ACS Omega 2020, 5, 14611−14618

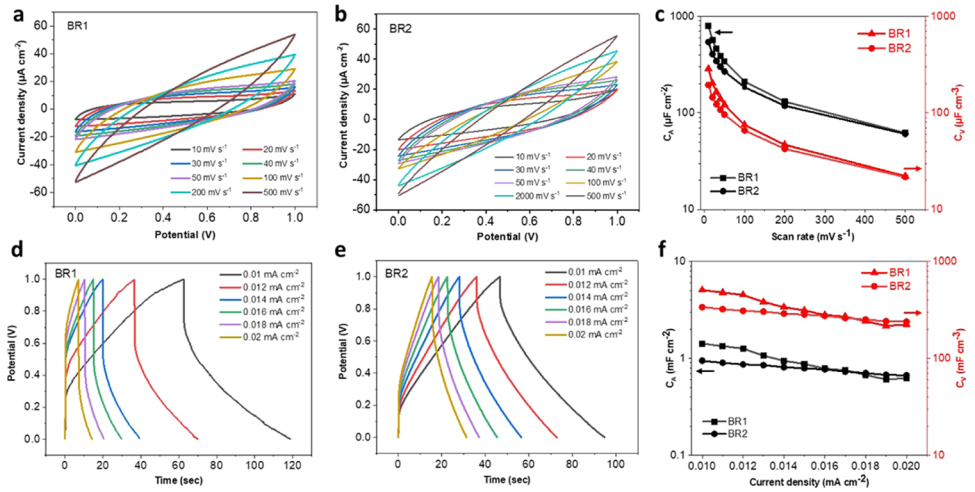

Figure 6. Electrochemical performance of LIG-80/PDMS-SC under bending. (a, b) CV curves obtained at different scan rates for BR1 and BR2, respectively. (c) Specific areal and volumetric capacitances as a function of scan rate for BR1 and BR2. (d, e) CD curves obtained at different current densities at BR1 and BR2, respectively. (f) Specific areal and volumetric capacitances as a function of current density for BR1 and BR2.

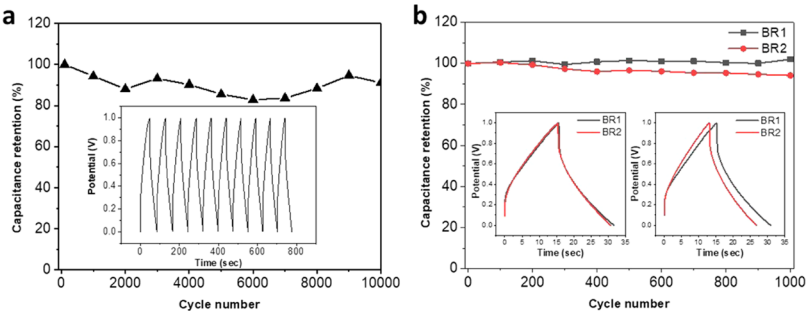

Figure 7. Cyclic stability of LIG-80/PDMS-SC based on CD analysis at a current density of 0.02 mA cm^{-2}: (a) 10 000 cycles without bending stress and (b) 1000 cycles for BR1 and BR2. The inset in (a) displays the first 10 CD cycles. The insets in (b) show a comparison of the first (left) and last (right) cycles for BR1 and BR2.

densities for LIG-80/PDMS were presented by a Ragone plot (Figure S4). When the current density was increased from 0.01 to 0.02 mA cm^{-2}, the energy density decreased from 3.13 × 10^{-7} to 1.52 × 10^{-7} Wh cm^{-2}, while the power density increased from 1.38 × 10^{-5} to 2.5 × 10^{-5} W cm^{-2}. These results are comparable to or even higher than those of graphene-based electrode for flexible/stretchable solid-state supercapacitors (Table S1).[34,35] Further improvement on power and energy densities would be expected by transferring more LIG to PDMS, doping heteroatom to LIG, or coating LIG with conductive materials. As laser power significantly affects the LIG quality, we also compared flexible SCs fabricated using LIG generated at various laser powers. Although decent capacitive behavior was observed with other LIG/PDMS electrodes, their performances were far below that of LIG-80/PDMS (Figure S5). The higher electrochemical behavior of LIG-80/PDMS should be attributed to the much lower sheet resistance and the higher quality of LIG-80 as characterized above.

From a practical point of view, flexible SCs should be deformed without significantly sacrificing performance. The electrochemical performance of LIG-80/PDMS-SC was thus further investigated under bending deformation. The device was held in place using a standard Vernier caliper for CV and CD analyses following the same procedures for no bending deformation (Figure S1). The bending radii of the two positions were 0.725 and 1.1825 cm, denoted as BR1 and BR2, respectively. The device with both bending radii showed good capacitive behaviors (Figure 6a,d). The high interfacial adhesion between the LIG-80 and PDMS provides high stability, which enabled the fabricated SCs to bear mechanical stress under bending deformation.[36,37] Even at the highest scan rate (500 mV S^{-1}), the CV curve still remained quasi-rectangular (Figure 6a). Similarly, the near-triangular shape of CD curves was also maintained at a higher current density (Figure 6d). Moreover, mechanical deformation under modest bending strain did not significantly affect specific capacitance. At the scan rate of 10 mV s^{-1}, the device with BR1 gave a C_A value of 800 μF cm^{-2}, which was similar to that obtained without bending. However, at a higher bending radius (1.1825 cm), device capacitances were compromised when a lower scan rate or current density was applied (e.g., about 39% decrease in C_A at 10 mV s^{-1}) (Figure 6). It is interesting to note that at a higher scan rate or current density, the capacitances for both radii showed similar values. The rippling of LIG electrodes under bending should be a major reason for relatively compromised performance. The thickness of the electric double layer increased due to the rippling when the device bent, leading to reduced capacitance.[3,34]

The stability of the fabricated LIG-80/PDMS SCs was evaluated since the cycle life is another important property of SCs. The analysis was carried out through many CD cycles at a current density of 0.02 mA cm^{-2}. As shown in Figure 7a, the device without bending retained more than 91% of initial areal

https://dx.doi.org/10.1021/acsomega.0c01293
ACS Omega 2020, 5, 14611−14618

capacitance at the end of 10 000 CD cycles, indicating excellent electrochemical stability. The device showed even higher stability under bending stress. At the end of 1000 cycles of CD analysis, the device displayed no loss of capacitance for BR1 and more than 94% of capacitance retention for BR2 (Figure 7b).

CONCLUSIONS

In summary, we demonstrated a facile synthesis of graphene from kraft lignin via laser writing and its application for flexible SCs. Laser writing photothermally converted kraft lignin into few-layered graphene. High-quality graphene with the least sheet resistance was obtained at 80% laser power. The three-dimensional porous structure allowed proper infiltration of LIG by PDMS to facilitate LIG transfer. The SC fabricated using LIG/PDMS as a soft electrode displayed good capacitive behaviors and excellent cyclic stability even under mechanical deformation with bending stress. Overall, the present work showed the successful fabrication of LIG from kraft lignin and its use for flexible energy storage device. It can also be envisioned that the LIG/PDMS electrode has high potential to be integrated with artificial skin and wearable electronic systems.

EXPERIMENTAL SECTION

Fabrication of Kraft Lignin/PEO Film and LIG. Softwood kraft lignin (supplied by Domtar Corporation) was used as a carbon precursor for LIG formation. A composite film comprising kraft lignin and poly(ethylene oxide) (PEO) (Polyox WSR 301, $M_W = 4 \times 10^6$) with a mass ratio of 4:3 was first fabricated following a procedure described in our prior study with some modification.[24] In brief, a PEO solution was prepared by dissolving 0.75 g of PEO into 40 mL of deionized water. One gram of kraft lignin was dissolved in 10 mL of 2 wt % NaOH solution and then mixed with the PEO solution. The mixture was continuously stirred to form a homogeneous, dark brown solution and then cast onto a plastic Petri dish (9 cm in diameter) for the film formation. After air drying, the film was peeled off from the Petri dish and cut into desired dimensions for laser processing.

DLW was conducted using a 40 W 10.6 μm CO_2 laser (H-Series 20 × 12 Desktop laser, Full Spectrum, Las Vegas, NV). All of the lasing tests were carried out under ambient condition with a beam size of 100 μm at a "z" distance of 2 mm, an image density of 1000 pulses per inch (PPI), and a scan rate of 20 cm s^{-1}. Laser power ranging from 30 to 90% of a 40 W laser power setting was applied to irradiate the above-prepared lignin/PEO film in a dimension of 1 cm × 1 cm. The LIG fabricated was denoted as LIG-X, where X stands for laser power percentage.

Fabrication of LIG/PDMS Electrodes and SCs. PDMS (Sylgard 184, Dow Corning) was first prepared by mixing PDMS agent A (silicon elastomer) and agent B (curing agent) with a mass ratio of 10:1 and then poured on top of an irradiated lignin/PEO film in an aluminum mold. The mold was then placed under vacuum in a desiccator for 10−15 min to remove air bubbles. It was further placed at 60 °C in a convection oven overnight to allow for the curing of PDMS. The LIG/PDMS composite was finally fabricated by peeling it off from the lignin/PEO film. The schematic diagram for the composite fabrication process is shown in Figure 1a.

An LIG/PDMS electrode was assembled as follows. Silver paint (Pellco colloidal paint, Catalog No. 16034, Ted Pella) was first applied to the edges of LIG transferred to PDMS. Conductive copper tape was applied to one side of the silver paint, serving as an extended current collector. Kapton PI tape was then applied to silver paint and portion of copper tape to avoid short circuiting. After assembly, one electrode was coated with gel electrolyte consisting of PVA (M_W = 124 000−186 000) and H_2SO_4 (1 M) and stacked with another electrode to form an SC in a sandwich structure (Figure 1b). The fabricated SC was placed under vacuum in a desiccator to allow gel electrolyte to become completely dry. The dried PVA in the electrolyte served as a separator between the two LIG/PDMS electrodes. The electrochemical performance of the fabricated SCs was evaluated by attaching the extended copper tape to an electrochemical workstation. The electrochemical analysis was described in detail in the Supporting Information.

Characterization of LIG. SEM was used to examine the morphology and thickness of the fabricated LIG and LIG/PDMS composite. SEM imaging was performed using an FEI Quanta 600 FEG environmental scanning electron microscope equipped with a Bruker Quantax 200 Silicon Drift Detector and operated at 15 kV and 100 pA. The film samples cut into small dimensions were mounted onto an adhesive SEM sample holder for imaging. TEM imaging was performed using an FEI Tecnai F30 300 kV transmission electron microscope. LIG powder scraped off from laser-irradiated films was sonicated in ethanol for 5 min and then transferred onto a C-flat TEM grid for TEM imaging.

Raman spectra were acquired on a Raman spectrometer (Reinshaw inVia) at 633 nm. The crystalline size of graphitic carbon in the a axis (L_a) was calculated based on the intensity ratio of G to D peaks (I_G/I_D) shown in Raman spectra, with the expression given in the Supporting Information. The chemical composition of LIG was analyzed using X-ray photoelectron spectroscopy (XPS), which was performed using a Kratos Axis 165 Photo Electron Spectroscopy system under a vacuum level of 3.0×10^{-8} Torr. XPS survey spectra were acquired in a step size of 0.5 eV with a pass energy of 160 eV. High-resolution spectra of C 1s were obtained in a step size of 0.1 eV with a pass energy of 20 eV. The sheet resistance of the LIG film was measured using a four-probe bridge resistivity system (Keithley 2400 Series SourceMeter). LIG embedded on lignin/PEO films was used for characterization, unless stated otherwise.

ASSOCIATED CONTENT

Supporting Information

The Supporting Information is available free of charge at https://pubs.acs.org/doi/10.1021/acsomega.0c01293.

Characterization; electrochemical analysis; comparison of graphene-based flexible SCs (Table S1); XPS spectra and functionality revealed by high-resolution C 1s XPS (Figure S2); SEM images of the remaining LIG-80 structure after peeling off (Figure S3); Ragone plots of LIG-80/PDMS-SC (Figure S4); and electrochemical analysis of LIG/PDMS-SC (Figure S5) (PDF)

AUTHOR INFORMATION

Corresponding Author

Caixia Wan − *Department of Biomedical, Biological, and Chemical Engineering, University of Missouri, Columbia, Missouri 65211, United States;* orcid.org/0000-0001-5490-

https://dx.doi.org/10.1021/acsomega.0c01293
ACS Omega 2020, 5, 14611−14618

7490; Phone: +1 573 884 7882; Email: wanca@missouri.edu; Fax: +1 573 884 5650

Authors

Faisal Mahmood − *Department of Biomedical, Biological, and Chemical Engineering, University of Missouri, Columbia, Missouri 65211, United States; Department of Energy Systems Engineering, University of Agriculture Faisalabad, Faisalabad 38000, Pakistan;* orcid.org/0000-0003-4833-9225

Hanwen Zhang − *Department of Biomedical, Biological, and Chemical Engineering, University of Missouri, Columbia, Missouri 65211, United States*

Jian Lin − *Department of Mechanical and Aerospace Engineering, University of Missouri, Columbia, Missouri 65211, United States;* orcid.org/0000-0002-4675-2529

Complete contact information is available at: https://pubs.acs.org/10.1021/acsomega.0c01293

Author Contributions

The manuscript was written through contributions of all authors. All authors have given approval to the final version of the manuscript.

Notes

The authors declare no competing financial interest.

■ ACKNOWLEDGMENTS

This work was supported by the National Science Foundation (grant no. 1933861). The authors also thank the support from the University of Missouri Electron Microscopy Core facility.

■ REFERENCES

(1) Li, L.; Lou, Z.; Chen, D.; Jiang, K.; Han, W.; Shen, G. Recent advances in flexible/stretchable supercapacitors for wearable electronics. *Small* **2018**, *14*, No. 1702829.

(2) Liu, L.; Feng, Y.; Wu, W. Recent progress in printed flexible solid-state supercapacitors for portable and wearable energy storage. *J. Power Sources* **2019**, *410-411*, 69−77.

(3) Zhang, L. L.; Zhao, X. Carbon-based materials as supercapacitor electrodes. *Chem. Soc. Rev.* **2009**, *38*, 2520−2531.

(4) Lu, Z.; Lin, X.; Zhang, J.; Dai, W.; Liu, B.; Mo, G.; Ye, J.; Ye, J. Ionic liquid/poly-L-cysteine composite deposited on flexible and hierarchical porous laser-engraved graphene electrode for high-performance electrochemical analysis of lead ion. *Electrochim. Acta* **2019**, *295*, 514−523.

(5) Zhang, L.; DeArmond, D.; Alvarez, N. T.; Malik, R.; Oslin, N.; McConnell, C.; Adusei, P. K.; Hsieh, Y.-Y.; Shanov, V. Flexible micro-supercapacitor based on graphene with 3D structure. *Small* **2017**, *13*, No. 1603114.

(6) Ran, F.; Yang, X.; Shao, L. Recent progress in carbon-based nanoarchitectures for advanced supercapacitors. *Adv. Compos. Hybrid Mater.* **2018**, *1*, 32−55.

(7) Raccichini, R.; Varzi, A.; Passerini, S.; Scrosati, B. The role of graphene for electrochemical energy storage. *Nat. Mater.* **2015**, *14*, 271.

(8) Huang, Y.; Liang, J.; Chen, Y. An overview of the applications of graphene-based materials in supercapacitors. *Small* **2012**, *8*, 1805−1834.

(9) Wang, Y.; Shi, Z.; Huang, Y.; Ma, Y.; Wang, C.; Chen, M.; Chen, Y. Supercapacitor devices based on graphene materials. *J. Phys. Chem. C* **2009**, *113*, 13103−13107.

(10) Ye, R.; James, D. K.; Tour, J. M. Laser-induced graphene: From discovery to translation. *Adv. Mater.* **2019**, *31*, No. 1803621.

(11) Lin, J.; Peng, Z.; Liu, Y.; Ruiz-Zepeda, F.; Ye, R.; Samuel, E. L. G.; Yacaman, M. J.; Yakobson, B. I.; Tour, J. M. Laser-induced porous graphene films from commercial polymers. *Nat. Commun.* **2014**, *5*, No. 5714.

(12) Ye, R.; James, D. K.; Tour, J. M. Laser-induced graphene. *Acc. Chem. Res.* **2018**, *51*, 1609−1620.

(13) Wang, C.; Xia, K.; Wang, H.; Liang, X.; Yin, Z.; Zhang, Y. Advanced carbon for flexible and wearable electronics. *Adv. Mater.* **2019**, *31*, No. 1801072.

(14) Lu, J. Y.; Zhang, X. X.; Zhu, Q. Y.; Zhang, F. R.; Huang, W. T.; Ding, X. Z.; Xia, L. Q.; Luo, H. Q.; Li, N. B. Highly tunable and scalable fabrication of 3D flexible graphene micropatterns for directing cell alignment. *ACS Appl. Mater. Interfaces* **2018**, *10*, 17704−17713.

(15) Luong, D. X.; Yang, K.; Yoon, J.; Singh, S. P.; Wang, T.; Arnusch, C. J.; Tour, J. M. Laser-induced graphene composites as multifunctional surfaces. *ACS Nano* **2019**, *13*, 2579−2586.

(16) You, R.; Liu, Y.-Q.; Hao, Y.-L.; Han, D.-D.; Zhang, Y.-L.; You, Z. Laser fabrication of graphene-based flexible electronics. *Adv. Mater.* **2020**, *32*, No. e1901981.

(17) Lamberti, A.; Clerici, F.; Fontana, M.; Scaltrito, L. J. A. E. M. A highly stretchable supercapacitor using laser-induced graphene electrodes onto elastomeric substrate. *Adv. Energy Mater.* **2016**, *6*, No. 1600050.

(18) Ye, R.; Chyan, Y.; Zhang, J. B.; Li, Y. L.; Han, X.; Kittrell, C.; Tour, J. M. Laser-induced graphene formation on wood. *Adv. Mater* **2017**, *29*, No. 1702211.

(19) Han, X.; Ye, R.; Chyan, Y.; Wang, T.; Zhang, C.; Shi, L.; Zhang, T.; Zhao, Y.; Tour, J. M. Laser-induced graphene from wood impregnated with metal salts and use in electrocatalysis. *ACS Appl. Nano Mater.* **2018**, *1*, 5053−5061.

(20) Chyan, Y.; Ye, R.; Li, Y.; Singh, S. P.; Arnusch, C. J.; Tour, J. M. Laser-induced graphene by multiple lasing: Toward electronics on cloth, paper, and food. *ACS Nano* **2018**, *12*, 2176−2183.

(21) Ragauskas, A. J.; Beckham, G. T.; Biddy, M. J.; Chandra, R.; Chen, F.; Davis, M. F.; Davison, B. H.; Dixon, R. A.; Gilna, P.; Keller, M.; Langan, P.; Naskar, A. K.; Saddler, J. N.; Tschaplinski, T. J.; Tuskan, G. A.; Wyman, C. E. Lignin valorization: Improving lignin processing in the biorefinery. *Science* **2014**, *344*, No. 1246843.

(22) Zhang, W. L.; Lei, Y. J.; Ming, F. W.; Jiang, Q.; Costa, P. M. F. J.; Alshareef, H. N. Lignin laser lithography: A direct-write method for fabricating 3d graphene electrodes for microsupercapacitors. *Adv. Energy Mater.* **2018**, *8*, No. 1801840.

(23) Wang, S.; Yu, Y.; Luo, S.; Cheng, X.; Feng, G.; Zhang, Y.; Wu, Z.; Compagnini, G.; Pooran, J.; Hu, A. All-solid-state supercapacitors from natural lignin-based composite film by laser direct writing. *Appl. Phys. Lett.* **2019**, *115*, No. 083904.

(24) Mahmood, F.; Zhang, C.; Xie, Y.; Stalla, D.; Lin, J.; Wan, C. Transforming lignin into porous graphene via direct laser writing for solid-state supercapacitors. *RSC Adv.* **2019**, *9*, 22713−22720.

(25) Hu, J.; Zhang, Q.; Lee, D.-J. Kraft lignin biorefinery: A perspective. *Bioresour. Technol.* **2018**, *247*, 1181−1183.

(26) Li, Y.; Ragauskas, A. J. Kraft lignin-based rigid polyurethane foam. *J. Wood Chem. Technol.* **2012**, *32*, 210−224.

(27) Yan, Q.; Zhang, X.; Li, J.; Hassan, E. B.; Wang, C.; Zhang, J.; Cai, Z. Catalytic conversion of Kraft lignin to bio-multilayer graphene materials under different atmospheres. *J. Mater. Sci.* **2018**, *53*, 8020−8029.

(28) Ferrari, A. C.; Meyer, J. C.; Scardaci, V.; Casiraghi, C.; Lazzeri, M.; Mauri, F.; Piscanec, S.; Jiang, D.; Novoselov, K. S.; Roth, S.; Geim, A. K. Raman spectrum of graphene and graphene layers. *Phys. Rev. Lett.* **2006**, *97*, No. 187401.

(29) Xu, Y.; Lin, Z.; Zhong, X.; Huang, X.; Weiss, N. O.; Huang, Y.; Duan, X. Holey graphene frameworks for highly efficient capacitive energy storage. *Nat. Commun.* **2014**, *5*, No. 4554.

(30) Zang, X.; Zhu, M.; Li, X.; Li, X.; Zhen, Z.; Lao, J.; Wang, K.; Kang, F.; Wei, B.; Zhu, H. Dynamically stretchable supercapacitors based on graphene woven fabric electrodes. *Nano Energy* **2015**, *15*, 83−91.

(31) Wu, Z. S.; Liu, Z.; Parvez, K.; Feng, X.; Müllen, K. J. A. M. Ultrathin printable graphene supercapacitors with AC line - filtering performance. *Adv. Mater.* **2015**, *27*, 3669−3675.

(32) Qi, D.; Liu, Z.; Liu, Y.; Leow, W. R.; Zhu, B.; Yang, H.; Yu, J.; Wang, W.; Wang, H.; Yin, S.; Chen, X. Suspended wavy graphene microribbons for highly stretchable microsupercapacitors. *Adv. Mater.* **2015**, *27*, 5559−5566.
(33) Song, W.; Zhu, J.; Gan, B.; Zhao, S.; Wang, H.; Li, C.; Wang, J. Flexible, stretchable, and transparent planar microsupercapacitors based on 3D porous laser-induced graphene. *Small* **2018**, *14*, No. 1702249.
(34) Gao, Y.; Zhou, Y. S.; Xiong, W.; Jiang, L. J.; Mahjouri-samani, M.; Thirugnanam, P.; Huang, X.; Wang, M. M.; Jiang, L.; Lu, Y. F. Transparent, flexible, and solid-state supercapacitors based on graphene electrodes. *APL Mater.* **2013**, *1*, No. 012101.
(35) Meng, Y.; Zhao, Y.; Hu, C.; Cheng, H.; Hu, Y.; Zhang, Z.; Shi, G.; Qu, L. All-graphene core-sheath microfibers for all-solid-state, stretchable fibriform supercapacitors and wearable electronic textiles. *Adv. Mater.* **2013**, *25*, 2326−2331.
(36) Wang, W.; Lu, L.; Xie, Y.; Mei, X.; Tang, Y.; Wu, W.; Liang, R. Tailoring the surface morphology and nanoparticle distribution of laser-induced graphene/Co_3O_4 for high-performance flexible micro-supercapacitors. *Appl. Surf. Sci.* **2020**, *504*, No. 144487.
(37) Wang, W.; Lu, L.; Xie, Y.; Yuan, W.; Wan, Z.; Tang, Y.; Teh, K. S. A highly stretchable microsupercapacitor using laser-induced graphene/NiO/Co_3O_4 electrodes on a biodegradable waterborne polyurethane substrate. *Adv. Mater. Technol.* **2020**, *5*, No. 1900903.

https://dx.doi.org/10.1021/acsomega.0c01293
ACS Omega 2020, 5, 14611−14618